Journal of Inflammation Research

Dovepress
open access to scientific and medical research

Open Access Full Text Article

ORIGINAL RESEARCH

VISTA Deficiency Exacerbates the Development of Pulmonary Fibrosis by Promoting Th17 Differentiation

Haiping Xie[1,*], Xuexin Zhong[1,*], Junlin Chen[2], Shuang Wang[1], Yuefang Huang[2], Niansheng Yang[1]

[1]Department of Rheumatology and Clinical Immunology, The First Affiliated Hospital, Sun Yat-Sen University, Guangzhou, 510080, People's Republic of China; [2]Department of Pediatrics, The First Affiliated Hospital, Sun Yat-Sen University, Guangzhou, 510080, People's Republic of China

*These authors contributed equally to this work

Correspondence: Niansheng Yang, Department of Rheumatology and Clinical Immunology, The First Affiliated Hospital, Sun Yat-sen University, 58 Zhongshan Second Road, Guangzhou, 510080, People's Republic of China, Tel +86-20-87755766 ext 8150, Email yangnsh@mail.sysu.edu.cn

Background: Interstitial lung disease (ILD), characterized by pulmonary fibrosis (PF), represents the end-stage of various ILDs. The immune system plays an important role in the pathogenesis of PF. V-domain immunoglobulin suppressor of T-cell activation (VISTA) is an immune checkpoint with immune suppressive functions. However, its specific role in the development of PF and the underlying mechanisms remain to be elucidated.

Methods: We assessed the expression of VISTA in CD4 T cells from patients with connective tissue disease-related interstitial lung disease (CTD-ILD). Spleen cells from wild-type (WT) or *Vsir*$^{-/-}$ mice were isolated and induced for cell differentiation in vitro. Additionally, primary lung fibroblasts were isolated and treated with interleukin-17A (IL-17A). Mice were challenged with bleomycin (BLM) following VISTA blockade or *Vsir* knockout. Moreover, WT or *Vsir*$^{-/-}$ CD4 T cells were transferred into *Rag1*$^{-/-}$ mice, which were then challenged with BLM.

Results: VISTA expression was decreased in CD4 T cells from patients with CTD-ILD. *Vsir* deficiency augmented T-helper 17 (Th17) cell differentiation in vitro. Furthermore, IL-17A enhanced the production of inflammatory cytokines, as well as the differentiation and migration of lung fibroblasts. Both VISTA blockade and knockout of *Vsir* increased the percentage of IL-17A-producing Th17 cells and promoted BLM-induced PF. In addition, mice receiving *Vsir*$^{-/-}$ CD4 T cells exhibited a higher percentage of Th17 cells and more severe PF compared to those receiving WT CD4 T cells.

Conclusion: These findings demonstrate the significant role of VISTA in modulating the development of PF by controlling Th17 cell differentiation. These insights suggest that targeting VISTA could be a promising therapeutic strategy for PF.

Keywords: VISTA, lung fibrosis, Th17 cells, IL-17A, fibroblast

Introduction

Interstitial lung disease (ILD) is characterized by the involvement of lung interstitium and alveolar spaces, presenting with abnormal proliferation of alveolar wall cells, infiltration of inflammatory cells, and interstitial fibrosis.[1] Pulmonary fibrosis (PF) represents the end-stage of various ILDs, characterized by fibroblast activation, progressive synthesis and deposition of extracellular matrix (ECM), ultimately leading to the destruction of lung architecture.[2] Despite this understanding, the precise mechanisms underlying PF remain unclear. Therefore, a more thorough exploration of PF pathogenesis may reveal novel therapeutic targets for anti-fibrotic treatment.

Recently, researchers have uncovered various functions of profibrotic cytokines in the pathogenesis of PF. Interleukin-17A (IL-17A) secreted by T-helper 17 (Th17) cells has been identified as a key promoter of PF development.[3–6] The frequency of IL-17A^{+}CD4^{+} T cells is expanded in ILD patients.[7,8] In Bleomycin (BLM)-induced PF, IL-17A has been found to enhance neutrophil accumulation and exacerbate PF progression. Conversely, blockade of IL-17A has been shown to alleviate lung

Received: 9 January 2024
Accepted: 30 May 2024
Published: 19 June 2024

Graphical Abstract

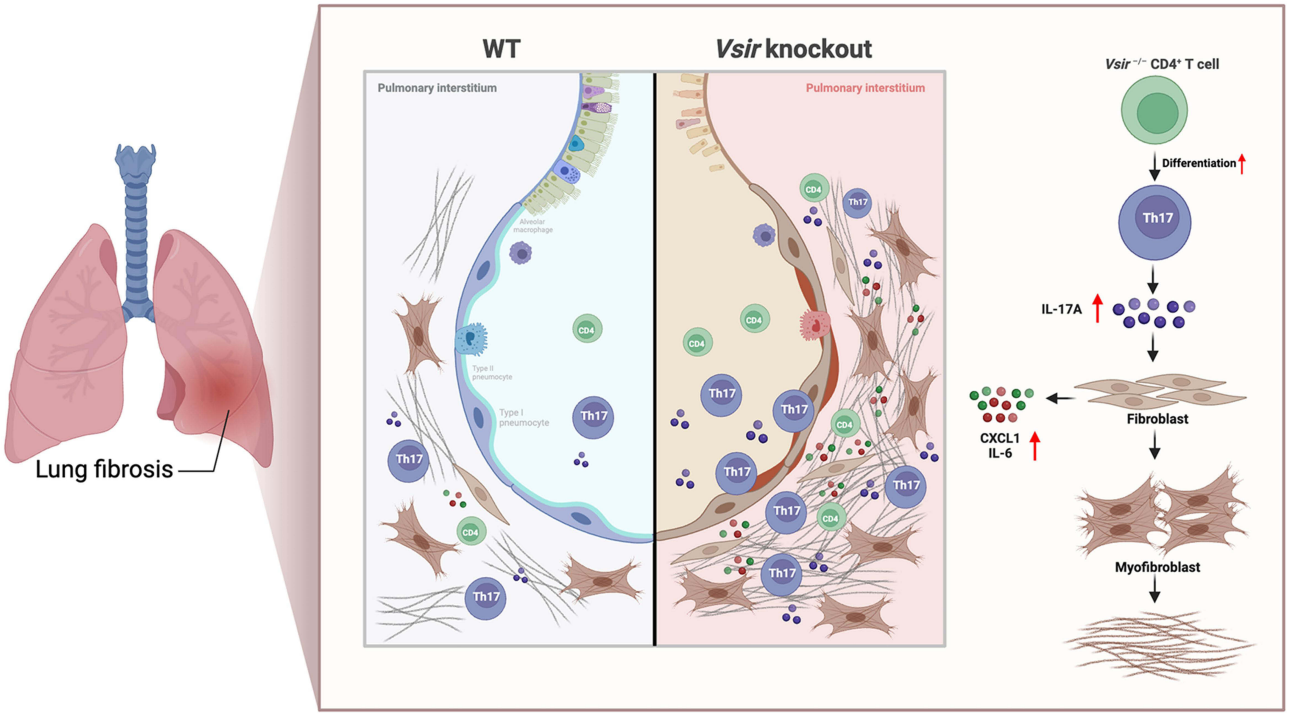

inflammation and fibrosis.[6,9,10] Additionally, research has demonstrated that IL-17A enhances collagen synthesis and secretion, promotes epithelial–mesenchymal transition, and suppresses epithelial cell autophagy, all contributing to the exacerbation of PF.[11] Despite these findings, the molecules and specific mechanisms regulating IL-17A secretion by Th17 cells in the context of PF remain elusive, highlighting the need for further research.

T cells are involved in PF by secreting numerous profibrotic and inflammatory cytokines, contributing to the subsequent process of fibroblast activation and ECM deposition.[12–14] Immune checkpoints such as PD-1, TIGIT and LAG3 are known to regulate the activation, differentiation and cytokine secretion of T cells.[15–19] V-domain immunoglobulin suppressor of T cell activation (VISTA), a recently identified negative immune checkpoint, is predominantly expressed in immune cells, with the highest expression in myeloid cells, followed by naive T cells (T_N) and forkhead box protein P3 (Foxp3) positive regulatory T cells (Treg).[20] VISTA is a promising target in cancer immunotherapy for drug-resistant cancers, playing a dual role as a ligand and a coinhibitory receptor in cancer progression.[21–23] Furthermore, studies have shown that VISTA is involved in the development of acute hepatitis,[24] asthma,[25] graft-versus-host disease[26] and lupus nephritis,[27] mainly through modulating the functions of immune cells, especially CD4 T cells. Additionally, VISTA expression on T_N cells and Treg cells made it eligible to modulate T cell quiescence and activation.[28–30] Although VISTA has been implicated in the pathogenesis of various diseases by regulating T cell functions, its role in the process of PF remains unknown.

In this study, we observed downregulation of VISTA expression in CD4 T cells from patients with connective tissue disease-related interstitial lung disease (CTD-ILD). In vitro experiments demonstrated that *Vsir* deficiency augmented Th17 cell differentiation. Furthermore, IL-17A enhanced the production of inflammatory cytokines, as well as the differentiation and migration of lung fibroblasts. Blockade of VISTA or deletion of *Vsir* resulted in enhanced Th17 cell differentiation and exacerbated BLM-induced PF. Additionally, *Rag1*$^{-/-}$ mice that received *Vsir*$^{-/-}$ CD4 T cells exhibited enhanced Th17 differentiation and worsened PF compared with those that received wild type (WT) CD4 T cells. Collectively, our study reveals a novel mechanism by which VISTA controls Th17 differentiation during lung fibrosis.

Material and Methods

Human Subjects

Patients diagnosed with CTD according to the diagnostic criteria of different types of CTDs, accompanied by diagnostic evidence from typical symptoms and physical signs, lung function test results, and high-resolution CT scans of ILD were included in our study from the First Affiliated Hospital, Sun Yat-sen University. Age- and gender-matched healthy controls (HCs) were enrolled. The demographic and clinical characteristics of human samples were unveiled in supplementary Table 1. The proposal for this study was approved by the Human Ethics Committee of The First Affiliated Hospital, Sun Yat-sen University ([2021]824). Informed consent was obtained from all participants. This study complied with the Declaration of Helsinki.

Mice

Vsir$^{-/-}$ mice and *Rag1*$^{-/-}$ mice of C57BL/6 background were purchased from GemPharmatech (Nanjing, China) and fed under specific pathogen-free conditions at the Experimental Animal Center of Sun Yat-sen University. All mice were maintained in a 12:12 h light/dark cycle environment with enough food and water. WT mice of C57BL/6 background were purchased from GemPharmatech (Nanjing, China). The animals selected in this study were all male. The approval of the research protocol was obtained from the Ethics Committee of the Laboratory Animal Center of Sun Yat-sen University (2022000686), and all operations were consistent with the guidelines of the National Institutes of Health Guide for Care and Use of Animals.

BLM-Induced Murine Model

BLM-induced PF mouse model was generated as previously described.[31] Briefly, age- and weight-matched male mice between 8 and 10 weeks old were selected in this study. Mice were anesthetized by intraperitoneal injection of 1% sodium pentobarbital, and surgical procedures were performed to expose the trachea. BLM (MCE, #HY-17565A) in 50ul LPS-free PBS (2 mg/kg) was injected into the trachea of mice. To implement the VISTA blockade treatment, mice received intraperitoneal administration of either anti-VISTA antibody (BioXcell, #BE0310) or isotype antibody every 3 days, starting at day 7 after the BLM instillation. The mice's weights were recorded throughout the disease progression, and on day 21, after a single intratracheal BLM administration, the mice were euthanized under deep anesthesia.

Peripheral blood mononuclear cells (PBMCs) Isolation

Human whole blood samples were collected in lithium heparin tubes, and PBMCs were isolated using Lymphoprep (STEMCELL Technologies). Briefly, PBMCs were separated by density gradient centrifugation and then washed with PBS twice. Resuspended PBMCs in freezing medium containing RPMI 1640 medium (Gibco), FBS (Procell) and DMSO (Asegene) were preserved in a −80 ˚C freezer overnight and then transferred to liquid nitrogen for further analysis.

Flow Cytometry Analysis

PBMCs separated from CTD-ILD patients and HCs were used for further flow cytometry analysis. For surface staining, PBMCs were labeled with PE/Cyanine7 anti-CD3 (1:100, clone #300316; BioLegend), Alexa Fluor® 647 anti-CD4 (1:100, clone #300520; BioLegend), PerCP anti-CD8 (1:100, clone #344708; BioLegend), Brilliant Violet 785™ anti-CD14 (1:150, clone #301840; BioLegend), Pacific Blue™ anti-CD56 (1:100, clone #318326; BioLegend), Brilliant Violet 711™ anti-CXCR5 (1:150, clone #356934; BioLegend), Brilliant Violet 605™ anti-C-C chemokine receptor type 6 (CCR6) (1:150, clone #353420; BioLegend), Brilliant Violet 510™ anti-CXCR3 (1:150, clone #353726; BioLegend), PE-anti-VISTA (1:100, clone #12-1088-41; eBioscience), APC/Cyanine7 anti-CCR7 (1:150, clone #353212; BioLegend), FITC anti-CD45RA (1:100, clone #304106; BioLegend), and Zombie Yellow™ Fixable Viability Kit (1:100, clone #423104; BioLegend) at 4 ˚C for 30 min. After which, cells were washed with PBS and then centrifuged twice. Surface makers of resuspended cells were analyzed by Cytek™ AURORA (Cytek Biosciences).

For murine lungs and draining lymph nodes analysis, single-cell suspensions were first incubated with ionomycin (500 ng/mL; Sigma-Aldrich), PMA (50 ng/mL; Sigma-Aldrich), and brefeldin A (5 mg/mL; SigmaAldrich) for 4.5 h. Subsequently, stimulated cells were stained with anti-CD45 (1:100, clone #103108; BioLegend), anti-CD3 (1:100, clone #100216; BioLegend), anti-CD8 (1:100, clone #100706; BioLegend), and washed with PBS. Cells were then

suspended with Fixation/Permeabilization solution (BD Biosciences) for fixation and permeabilization at 4 ˚C for 30 min and washed with Perm/Wash Buffer (BD Biosciences). Cells were stained with anti-IL-17A (1:50, clone #506916; BioLegend), anti-interferon-γ (IFN-γ) (1:50, clone #505702; BioLegend), anti-tumor necrosis factor-α (TNF-α) (1:50, clone #506304; BioLegend). Additionally, cells were stained with anti-Foxp3 (1:50, clone #320012; BioLegend) after permeabilization procedures with Foxp3 Staining Set (eBioscience). Finally, suspended cells were analyzed by Attune® NxT (ThermoFisher), and FlowJo software (Tree Star, USA) was used to analyze cytometry data.

Histology and Immunohistochemistry of Mice Lung

The left lobe of lung was excised and fixed with 4% paraformaldehyde. Lung sections (4 μm) were subsequently prepared for further staining. The paraffin-embedded lung sections were subjected to hematoxylin and eosin (H&E) staining, and the Ashcroft score was determined following established criteria.[32] The Ashcroft score for 10 images from each section was independently calculated by two observers. The final score was derived by computing the average value. Lung sections were subsequently subjected to Masson's trichrome staining, and the extent of fibrosis was assessed by calculating the average area across 10 images for each section.

For the immunohistochemistry experiment, paraffin-embedded sections underwent dewaxing and rehydration, followed by antigen retrieval in antigen retrieval solution (PH = 6.0, 0.01 M citrate buffer). After which, lung sections were incubated with 3% hydrogen peroxide to inactivate endogenous peroxidase. Subsequently, lung sections were blocked with 5% BSA in PBS for 1 h at room temperature and consecutively incubated with alpha-smooth muscle actin (α-SMA) (1:300, Abcam, #ab5694) antibody at 4 ˚C overnight. Sections were washed with 0.1% Tween in PBS three times and stained with horseradish-peroxidase (HRP)-conjugated secondary antibody (1:500, Servicebio, #GB23303) for 1h at room temperature. Consequently, lung sections were washed with 0.1% Tween in PBS for three times and visualized with DAB (Servicebio, #G1212), and data were analyzed using Image J software (NIH, USA).

Lung Single Cell Isolation

Mice were euthanized through excessive anesthesia, and the thoracic cavity was opened. Mice's lungs were harvested after perfusion with PBS. Two lung lobes were collected from each mouse and subsequently sectioned into small pieces measuring 1 mm each. Lung tissues were sequentially suspended in PBS and processed using an automated tissue processor (GentleMACS). Finally, the tissue suspension was refined using a 70-mm cell strainer (BD, USA), and single lung cells were obtained by centrifugation at 1500 rpm for 5 min.

Adoptive Transfer

Mice were treated with excessive anesthesia, and spleens were harvested after disinfecting with alcohol. The cell suspension was filtered to remove debris, purified using red blood cell lysis solution (Sigma, USA) and washed by PBS. Immunomagnetic negative selection Mouse CD4 T cell Isolation Kit (STEMCELL Technologies) was used to enrich total CD4 T cell from spleen cells. For adoptive transfer procedures, WT and *Vsir*$^{-/-}$ total CD4 T cells were resuspended, counted and then transferred intravenously into *Rag1*$^{-/-}$ recipient mice. *Rag1*$^{-/-}$ mice were subsequently utilized to establish a model of BLM-induced lung fibrosis.

Cell Culture

Single spleen cells were collected following filtration through a 70-mm cell strainer, red blood cell lysis, and subsequent washing in PBS. Pooled spleen cells were counted and added into 96-well-plates containing anti-mouse CD3 (BioLegend, USA, 5 μg/mL), anti-mouse CD28 (BioLegend, USA, 2 μg/mL) and cytokines used for CD4 T cells differentiation in RPMI 1640 supplemented with 10% FBS and 1% penicillin-streptomycin (Gibco). For Th17 differentiation, culture medium was added with transforming growth factor beta 1 (TGF-β1) (2 ng/mL, PeproTech, #100-21-2), IL-6 (40 ng/mL, Sino Biological, #50136-MNAE), IL-1β (20 ng/mL, PeproTech, #211-11B-2), IL-23 (30 ng/mL, NovoProtein, #C03U), anti-mouse IFN-γ (5 ng/mL, BioLegend, #505702), and anti-mouse IL-4 (5 ng/mL, BioLegend, #504102). For Treg differentiation, culture medium was added with TGF-β1 (5 ng/mL, PeproTech, #100-21-2), IL-2 (10 ng/mL, Sino Biologic, #51061-MNAE-20), anti-mouse IFN-γ (5 ng/mL, BioLegend, #505702), and anti-mouse IL-4 (5 ng/mL, BioLegend, #504102). Spleen cells were

cultured for 4 days and then collected for flow cytometry analysis and real-time PCR analysis. Cells were stimulated with ionomycin, PMA and brefeldin A for 4.5 h and subsequently stained with Alexa Fluor® 700 anti-CD3 (1:100, clone #100216; BioLegend), FITC anti-CD8 (1:100, clone #100706; BioLegend), APC anti-IL17A (1:50, clone #512306; BioLegend), PE anti-CD44 (1:50, clone #103008; BioLegend) and Alexa Fluor® 647 anti-Ki67 (1:50, clone #151206; BioLegend) following fixation and permeabilization.

Isolation and Culture of Mice Primary Lung Fibroblasts

Mice primary lung fibroblasts were isolated as previously described.[33] Briefly, mice were disinfected with alcohol after excessive anesthesia. The thorax was opened, and the whole lung of mice was perfused with PBS and then detached. The fresh lung was rinsed with PBS to remove blood and then cut into small pieces in DMEM culture medium (Gibco). Lung pieces were rinsed with PBS again and added to a 10-cm dish containing DMEM, 10% FBS and 1% penicillin-streptomycin for 6–7 days of culture. Finally, the adherent fibroblasts were digested with trypsin (Thermo Fisher Scientific) and filtered to remove lung tissues before passage. Fibroblasts used in further analysis were in passage 2–4. Primary lung fibroblasts were cultured in DMEM supplemented with 10% FBS and 1% penicillin-streptomycin until they reached approximately 70% confluence. Recombinant mouse IL-17A (50 ng/mL, PeproTech, #210-17-5) was subsequently added into the culture system at different time intervals. After 24 hours of culture, fibroblasts were collected for immunoblotting analysis. Real-time PCR analysis was conducted at 12-hour, 24-hour, and 48-hour time points of culture.

Immunoblotting Analysis

Fibroblasts were harvested, and total proteins were extracted using radioimmunoprecipitation assay (RIPA) lysis buffer, containing 1% halt protease/phosphatase (Asegene). BCA assay kit (EpiZyme) was applied to measure protein concentration. Extracted proteins were subjected to SDS-polyacrylamide gel electrophoresis (SDS-PAGE), followed by polyvinylidene difluoride membrane (Millipore). Membranes were incubated with 5% BSA in TBS including 0.1% Tween and then incubated with primary antibody against a-SMA (1:300, Abcam, #ab5694) and GAPDH (1:10000, Cell Signaling Technology, #D16H11) at 4 °C overnight. Specific anti-rabbit secondary antibody was used to testify the primary antibody and visualized by chemiluminescence Western blot imaging system (Amersham™ ImageQuant™ 800, Japan).

Wound-Healing Assay

Fibroblasts were collected and seeded into 12-well-plates to form a monolayer, and scratch was created using pipette tips. Non-adherent cells were removed with PBS three times, and serum-free DMEM was added to plates for further culture with or without IL-17A (50ng/mL, PeproTech, #210-17-5) administration. Wounds were noted at 12 hour and 24 hour by light microscope, and wound size was analyzed through ImageJ software.

Real-Time PCR

The TRIzol reagent (Invitrogen, USA) was applied to extract total RNA of cells, and the complementary DNA was generated through reverse transcription procedure using Evo M-MLV RT Premix (Accurate Biology, China). SYBR Green Chemistry (Accurate Biology) was used in real-time PCR process, and subsequently the complementary DNA was subjected to an amplification procedure, which involved an initial denaturation step at 95 °C for 30s, followed by 35 cycles of amplification at 95 °C for 5 s and annealing at 60 °C for 30s, concluding with elongation. Transcripts for genes were relative to *Gapdh* transcripts, and primers used for real-time PCR were shown in Supplementary Table 2.

RNA-Seq Analysis

Publicly available RNA-sequencing datasets related to PF were acquired from GEO datasets (accession codes: GSE213001, GSE150910, GSE93606). Differential gene expression was assessed utilizing the DESeq2 R package (version 1.28.1) through a moderated *t*-test with the Benjamini–Hochberg method. Criteria for significance were set at adjusted $p < 0.05$ and |log2 (fold change)| >1. Subsequently, gene set enrichment analysis (GSEA) and gene ontology (GO) analyses were conducted using the clusterProfiler R package (version 4.1.0). Pathways were deemed significantly enriched if the *p*-values, corrected for multiple hypothesis testing with the Benjamini–Hochberg method, were less than

0.05. The gene read count data were analyzed and visualized using R (version 4.0.5) and RStudio (integrated development for R).

Statistics

GraphPad Prism 9.0. Software was used to analyze data in the current study. Student's *t*-test was used in group comparison, and Pearson's correlation coefficient was utilized in correlation analysis. All data were presented as mean ± SEM, and we think it significant when $p<0.05$. *$p < 0.05$, **$p < 0.01$, ***$p < 0.001$, ****$p < 0.0001$.

Results

VISTA Expression is Downregulated in Patients with PF

To delineate the expression level of VISTA during PF, we first searched for and reanalyzed publicly available bulk RNA-seq data from HCs and patients with idiopathic pulmonary fibrosis (IPF). We observed that *VSIR* mRNA expression was dramatically lower in IPF patients compared to HCs (Figure 1A, GSE213001 and GSE150910). Additionally, we analyzed VISTA expression on PBMCs of CTD-ILD patients and HCs. Human PBMCs were subjected to flow cytometry, and a representative gating strategy was depicted for the classification of different cell subsets (Supplementary Figure 1A). We found that VISTA expression was significantly lower on CD4 T cells and NK cells from patients with PF compared to that from HCs. No significant difference in VISTA expression was noted on CD8 T cells, NKT cells, and monocytes between patients with CTD-ILD and HCs (Figure 1B and C). These results suggest that decreased VISTA expression on CD4 T cells appears to be involved in the development of PF. To further examine VISTA expression within CD4 T cell subsets, we classified CD4 T cells into four types based on the surface expression of CD45RA and CCR7, containing T_N cells ($CD45RA^+CCR7^+$), central memory T (T_{CM}) cells ($CD45RA^-CCR7^+$), effector memory T (T_{EM}) cells ($CD45RA^-CCR7^+$) and terminally differentiated T (T_{EMRA}) cells ($CD45RA^+CCR7^-$). VISTA expression was noted to be decreased on T_N and T_{EMRA} subsets in CTD-ILD samples compared to HCs. However, no difference in VISTA expression on T_{CM} and T_{EM} was observed (Figure 1D and E).

To investigate the impact of VISTA expression on the disease activity of patients with CTD-ILD, we analyzed the spirometry data of these patients and performed the correlation study between the percentage of $CD4^+VISTA^+$ cells and pulmonary function. The correlation study results revealed that the percentage of $CD4^+VISTA^+$ T cells was positively correlated with forced vital capacity (FVC) and total lung capacity (TLC), while no correlation was found between the percentage of $CD4^+VISTA^+$ T cells and the diffusing capacity of the lung for carbon monoxide (DLCO) (Figure 1F), suggesting a protective role of VISTA in the development of PF. Together, these findings indicate the relevance between VISTA down-regulation on CD4 T cells and PF development.

Vsir Deficiency Promotes CD4 T Cell Polarization Towards Th17 in vitro

We have observed the down-regulation of VISTA in PF and addressed the relevance between the percentage of $CD4^+VISTA^+$ T cells and lung function. Given the important role of IL-17A in PF, we focused on the study that how VISTA impacts the differentiation of CD4 T cells into Th17 cells in vitro. Interestingly, flow cytometry analysis revealed that IL-17A expression was notably higher in CD4 T cells from *Vsir*$^{-/-}$ mice compared with WT mice. However, the percentages of $Foxp3^+$ cells were similar between WT and knockout cells. In addition, no significant differences were observed between these two groups in terms of CD4 T cell proliferation and CD4 T cell activation as demonstrated by the percentages of Ki-67^+ and $CD44^+$ cells, respectively (Supplementary Figure 2A and B). Additionally, single cells were isolated from spleens of both *Vsir*$^{-/-}$ mice and WT mice, and then cultured in vitro under Th17 differentiation condition for 4 days. Subsequently, cells were collected, and total RNA was extracted for real-time PCR analysis. The results of real-time PCR revealed elevated mRNA levels of *Il17a* and *Il17f* in *Vsir*$^{-/-}$ mice (Supplementary Figure 2C). In conclusion, *Vsir* deficiency augments CD4 T polarization into Th17 cells in vitro.

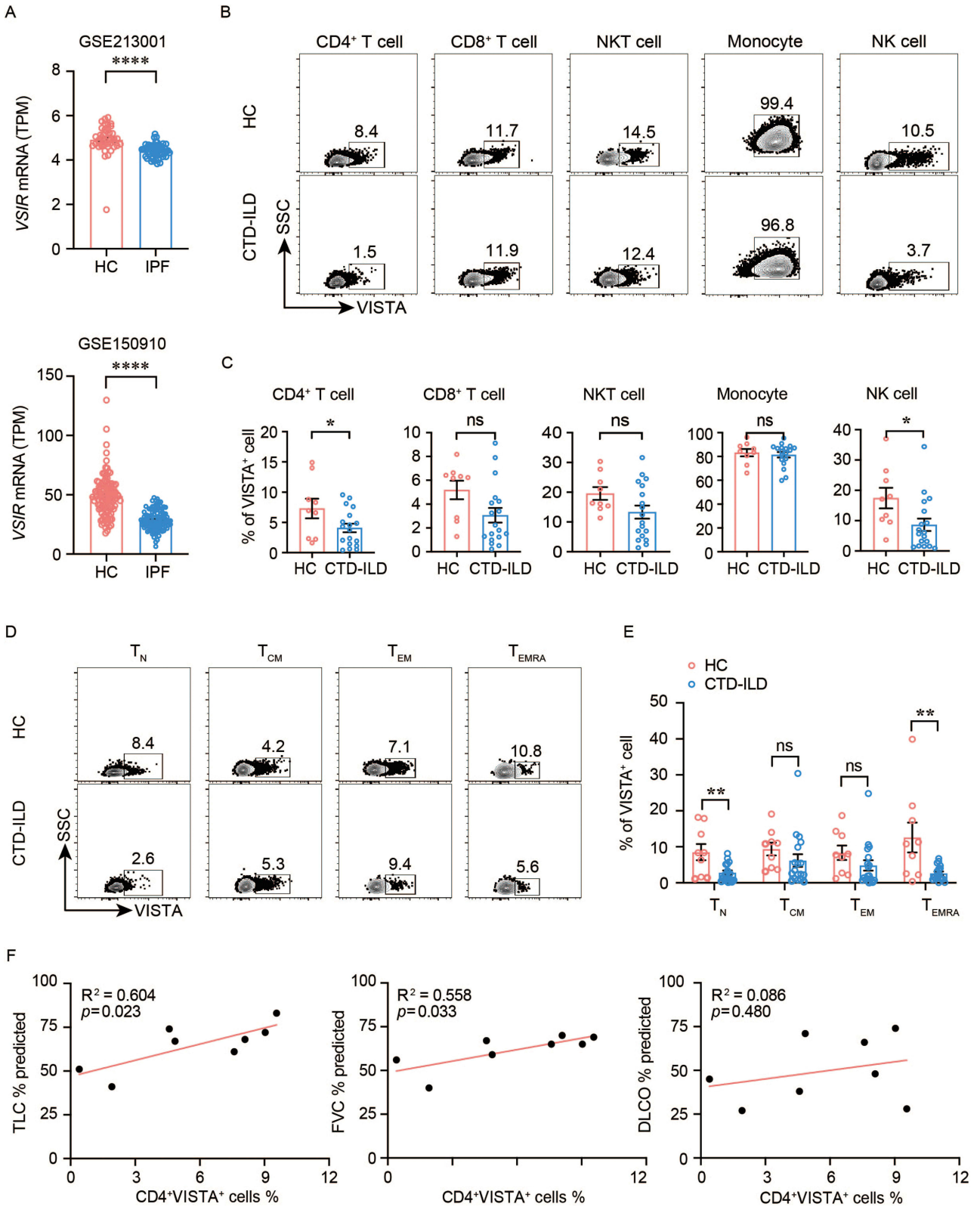

Figure 1 Decreased Vista expression in CD4 T cells in PF patients. (**A**) Bulk RNA-seq data of *VSIR* mRNA expression from IPF and HCs were obtained from public GEO datasets (GSE213001 and GSE150910). (**B**) Representative dot plots of Vista expression in different types of immune cells in PBMCs from CTD-ILD subjects and HCs. (**C**) Statistical results of the percentages of Vista in different cells (HC: n = 9; CTD-ILD: n = 18). (**D**) Typical gating images of Vista expression in four subsets of CD4 T cells. (**E**) Statistical analysis of the percentages of Vista expression in four subsets of CD4 T cells (HC: n = 9; CTD-ILD: n = 18). (**F**) The relationship between the percentage of $Vista^+CD4^+$ T cells and the data from pulmonary function test. Data are mean ± SEM. $*p < 0.05$, $**p < 0.01$, $****p < 0.0001$ by Student's *t* test. Correlation was done by Pearson's correlation coefficient.

The Involvement of IL-17 Signaling Pathway in PF Development

To further explore the involvement of IL-17A in the process of PF, we searched for and reanalyzed publicly available bulk RNA-seq data. Mechanistically, the result of GSEA indicated that the IL-17 signaling pathway was markedly upregulated and enriched in patients of IPF (Supplementary Figure 3A, GSE150910). In addition, we further analyzed the correlation between *IL17A* mRNA expression and typical published markers[34,35] of fibrosis in IPF patients. Intriguingly, *IL17A* mRNA expression was positively correlated with collagen type I alpha 1 (*COL1A1), COL3A1*, matrix metallopeptidase 2 (*MMP2*), tissue inhibitor of metalloproteinases 3 (*TIMP3*), chemokine (CC-motif) ligand 2 (*CCL2*) and *CCL17* (Supplementary Figure 3B, GSE93606). These data further highlight that the IL-17 signaling pathway and IL-17A are involved in PF development, which provides us a new clue to examine the role of VISTA-mediated IL-17A production by CD4 T cells in PF.

Th17 Cells Promote PF by Activating Fibroblasts

To gain a deeper insight into the role of Th17 cells during PF, we subjected differentially expressed genes (DEGs) extracted from a public data set to GO annotation (Supplementary Figure 3C, GSE150910). GO biological process analysis indicated that upregulated DEGs were significantly associated with cilium organization, microtubule-based movement, cilium assembly, and ECM organization. Additionally, changes in the cell component of upregulated DEGs were related to collagen-containing ECM. Moreover, changes in molecular function were also involved in ECM structural constituents. Given the important role of fibroblasts in PF,[33] we focused on the role of IL-17A on fibroblasts in PF. Primary lung fibroblasts were isolated from mice lungs according to the instruction published before,[33] and recombinant mouse IL-17A was added to culture system. We found that fibroblasts were activated by IL-17A, as indicated by significantly elevated expression of α-SMA in immunoblot analysis (Figure 2A and B), indicating a profibrotic phenotype of fibroblasts after IL-17A treatment. Furthermore, we found that IL-17A enhanced fibroblast migration ability in wound scratch assay, as depicted by obviously smaller wound size after 12-hour and 24-hour of IL-17A stimulation (Figure 2C and D). Gene expression of chemokine (C-X-C motif) ligand 1 (*Cxcl1*) and *Il6* were elevated in fibroblasts after 12-hour, 24-hour, and 48-hour of IL-17A stimulation (Figure 2E). Taken together, IL-17A is involved in PF by activating the differentiation, migration, and cytokine production of fibroblasts.

VISTA Blockade Accelerates PF Progression by Promoting Th17 Differentiation

To determine the role of VISTA in PF progression, we induced PF through a single-dose intratracheal instillation of BLM (Supplementary Figure 4A–E). To further elucidate the effect of BLM treatment on the expression of VISTA, spleen cells from both the PBS group and BLM group were isolated and subjected to flow cytometry. The data showed that VISTA expression on CD4 T cells was significantly lower in the BLM group compared to the PBS group (Supplementary Figure 4F). However, VISTA expression level remained similar in vitro culture after stimulation with either PBS or BLM for 2 days (Supplementary Figure 4G).

After BLM installation, the mice were then treated with 13F3 to block VISTA from day 7 (Figure 3A). Mice from both groups presented with weight loss 7 days after BLM induction, which was a typical manifestation of PF,[36–38] followed by a gradual gain of weight in the following course of the disease (Figure 3B). Importantly, mice received 13F3 injection manifested significantly more weight loss at day 17 and day 18 than mice received isotype antibody injection (Figure 3C and D). We observed that blockade of VISTA with 13F3 resulted in increased hemorrhagic spots compared to the control group. Moreover, more patchy dark-red lesions were observed in the lungs of mice treated with 13F3 antibody (Figure 3E). Accordingly, we assessed the severity of lungs from these two groups through H&E and Masson's trichrome staining. We observed increased immune cell infiltration and worsened PF in 13F3-treated group compared to isotype antibody-treated group (Figure 3F and H). These results were subsequently quantified using Ashcroft scoring[39] and by calculating the fibrotic areas (Figure 3G and I). Consistently, α-SMA expression was significantly higher in 13F3-treated group, visualized by immunohistochemistry staining of lung sections (Figure 3J and K). These findings suggest the involvement of VISTA in the progression of PF.

Based on the observations above, we next explored whether VISTA antagonism influences the differentiation of CD4 T cells. We detached draining lymph nodes and isolated single cells for further flow cytometry analysis. The data revealed that VISTA blockade enhanced IL-17A and IFN-γ production in BLM-induced CD4 T cells. Interestingly, TNF-

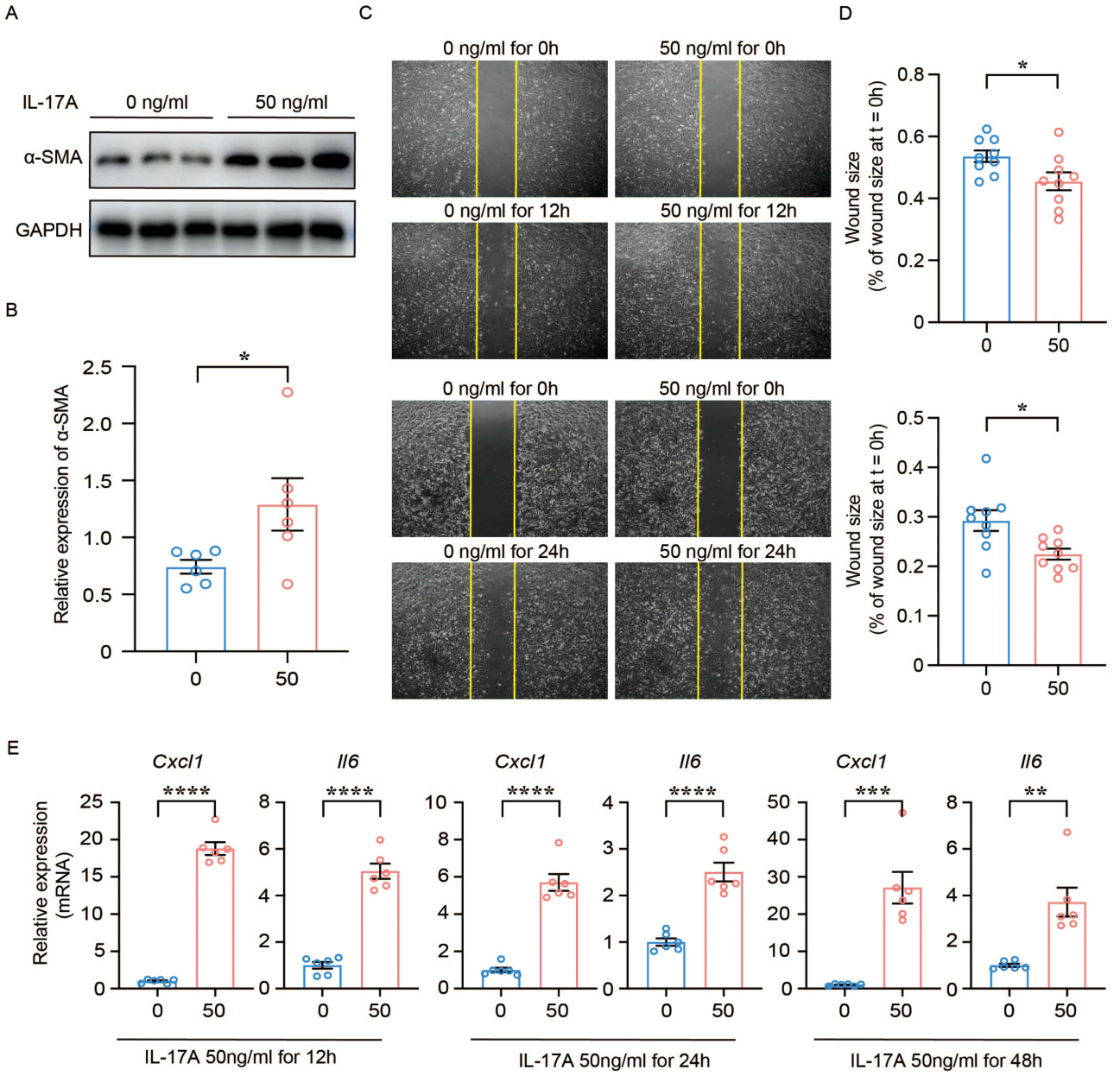

Figure 2 IL-17A activates the differentiation, migration, and cytokines production of fibroblasts (**A** and **B**) Primary lung fibroblasts were treated with or without IL-17A (50 ng/mL) for 24 h, and the expression of α-SMA was determined by immunoblot analysis. Representative bands were revealed. (**C** and **D**) Migration assay of fibroblasts under IL-17A stimulation. Representative images of migration assays at 12 h and 24 h after IL-17A stimulation were listed (**C**). Wound size was measured and counterplots were shown (**D**). (**E**) Cytokines expressions were detected by real-time PCR at 12 h, 24 h and 48 h after IL-17A treating, and counter plots were revealed. Data are mean ± SEM. *$p < 0.05$, **$p < 0.01$, ***$p < 0.001$, ****$p < 0.0001$ by Student's *t* test.

α and Foxp3 production in CD4 T cells were not changed by VISTA blockade (Figure 3L and M). Also, VISTA antagonism did not affect TNF-α and IFN-γ expression in CD8 T cells (Supplementary Figure 5A). In conclusion, VISTA blockade promotes CD4 T cells to differentiate into IL-17A-secreting T cells during BLM-induced lung fibrosis.

Vsir Deficiency Enhances Th17 Differentiation and Promotes BLM-Induced Lung Fibrosis

To evaluate the role of VISTA in PF development, we challenged WT and *Vsir*$^{-/-}$ mice with signal-dose BLM (Figure 4A). Mice from these two groups presented with a temporary weight loss, then went up gradually in the following days (Figure 4B). Additionally, *Vsir*$^{-/-}$ mice showed increased weight loss at day 16 post-BLM instillation (Figure 4C). Consistent with VISTA

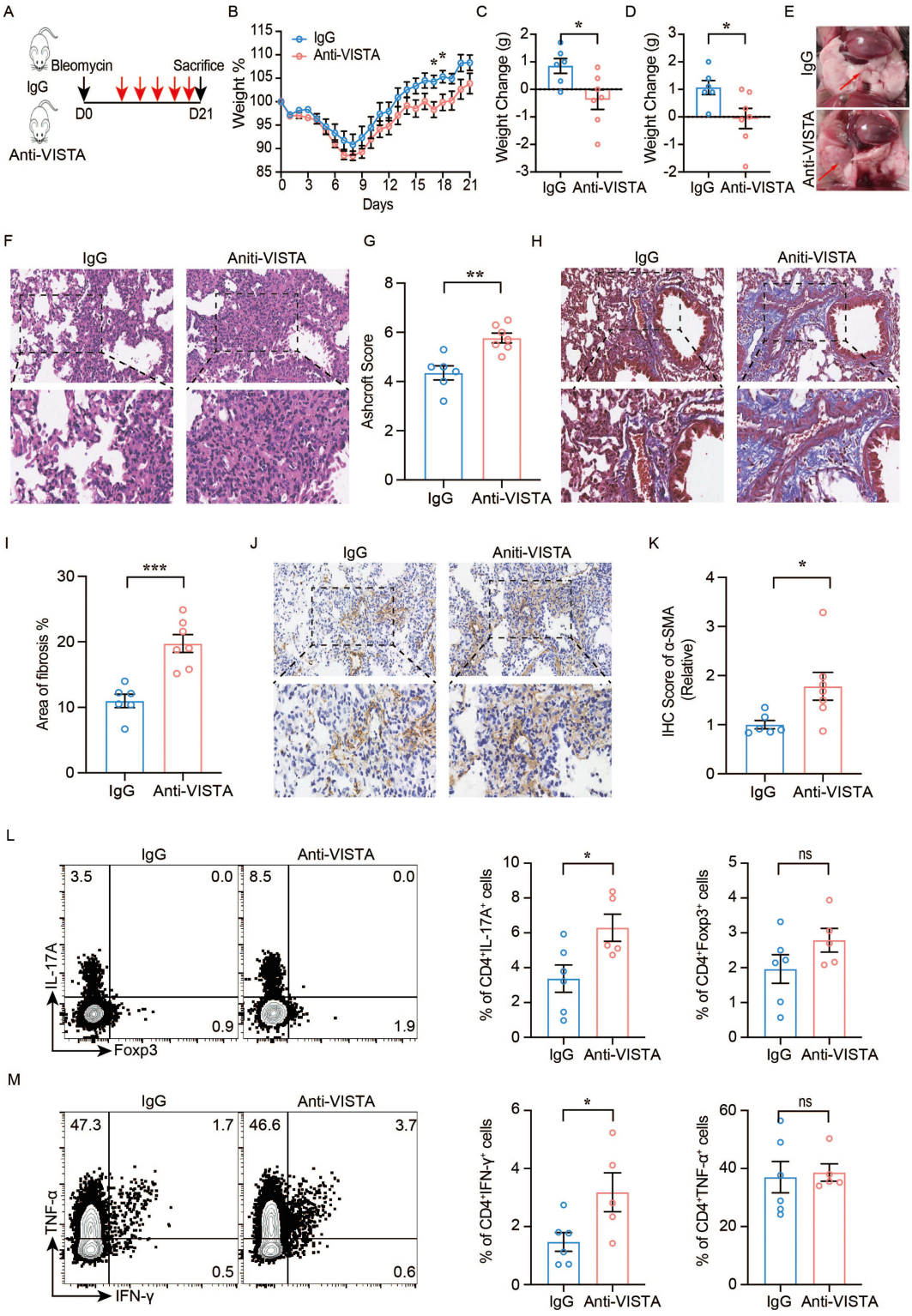

Figure 3 Anti-Vista antibody deteriorates BLM-induced lung fibrosis. (**A**) Schematic graph of the murine model in this experiment. WT mice receiving a single intratracheal injection of BLM underwent intraperitoneal instillation of anti-Vista antibody or isotype antibody every 3 days beginning at day 7 after BLM administration, and mice were sacrificed at day 21 (n = 6 in isotype antibody group, n = 7 in anti-Vista antibody group). (**B-D**) Weight changes of mice during the course of BLM-induced fibrosis (**B**), and the difference of weight changes between two groups at day 17 (**C**) and day 18 (**D**). (**E**) Images of lungs from mice in isotype antibody group (upper) or anti-Vista antibody group (lower) (The red arrow indicates the location of the lesion). (**F** and **G**) H&E staining of lung sections from mice (**F**), and Ashcroft score of each mouse in two groups (**G**). (**H** and **I**) Masson's trichrome staining of lung sections (**H**), and the difference in area of fibrosis between two groups (**I**). (**J** and **K**) Immunohistochemistry staining of lung sections (**J**), and relative score of α-SMA from each mouse (**K**). (**L** and **M**) Single cell suspensions of draining lymph nodes from mice in this experiment were prepared and subjected to flow cytometry analysis (n = 6 in isotype antibody group, n = 5 in anti-Vista antibody group). Representative gating strategies for cytokines expressions in CD4 T cells were listed. Cytokines IL-17A, Foxp3, TNF-α and IFN-γ expression levels in CD4 T cells were compared between two groups. Original magnification: ×20 (upper), ×40 (lower). Data are mean ± SEM. *$p < 0.05$, **$p < 0.01$, ***$p < 0.001$ by Student's t test.

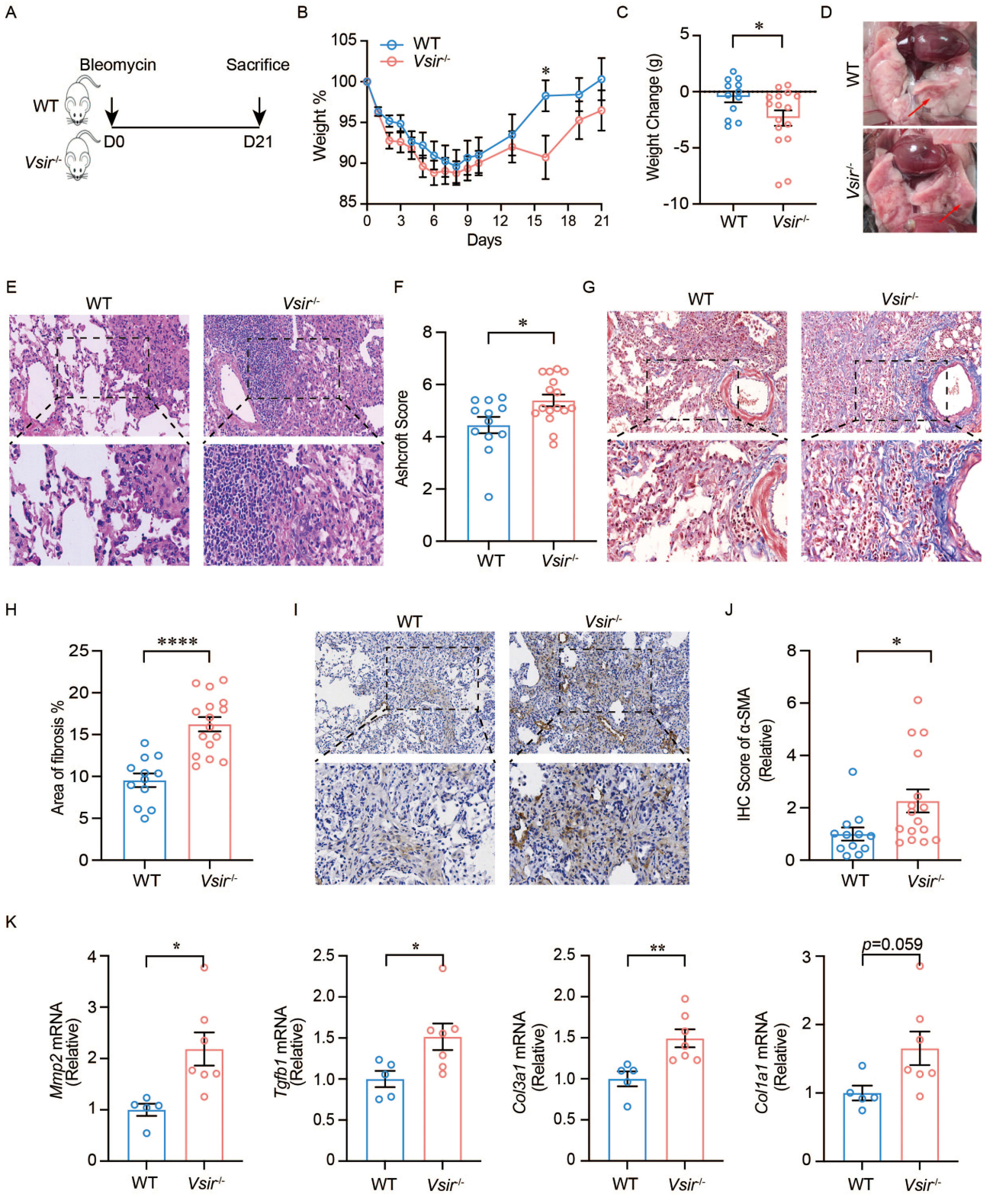

Figure 4 PF progression is aggravated in *Vsir*$^{-/-}$ mice compared to WT mice. (**A**) Schematic diagram of animal model. Age and weight-matched WT and *Vsir*$^{-/-}$ mice received single-dose administration of BLM at day 0, and were euthanized at day 21 (n =12 in WT group, n = 16 in *Vsir*$^{-/-}$ group). (**B** and **C**) Weight changes of WT and *Vsir*$^{-/-}$ mice were measured throughout the disease duration (**B**), and the difference in weight changes at day 16 was analyzed (**C**). (**D**) Representative images of lungs from WT (upper) and *Vsir*$^{-/-}$ (lower) mice (The red arrow indicates the location of the lesion). (**E–J**) Histological and immunohistochemistry analysis of mice lungs. H&E staining of fibrosis lung tissues (**E**), and Ashcroft scores were calculated (**F**). Masson's trichrome staining for each mouse (**G**), and areas of fibrosis were compared in two groups (**H**). Immunohistochemistry staining of α-SMA was performed for lung sections (**I**), and relative scores were determined (**J**). (**K**) Fibrosis markers expressions were detected by real-time PCR and counter plots were revealed. Original magnification: ×20 (upper), ×40 (lower). Data are mean ± SEM. *$p < 0.05$, **$p < 0.01$, ****$p < 0.0001$ by Student's *t* test.

blockade, knockout of *Vsir* led to increased bleeding sites in the lung. In addition, patchy dark-red lesions were increased in *Vsir*$^{-/-}$ mice (Figure 4D). Histological analysis of lung sections revealed a similar result. Lung sections were stained H&E and Masson's trichrome to evaluate cell infiltration and collagen accumulation, respectively, the data revealed that cell infiltration and collagen accumulation were notably increased in *Vsir*$^{-/-}$ mice compared to WT mice (Figure 4E–H). In addition, knockout of *Vsir* also elevated α-SMA expression in the lungs (Figure 4I and J). The mRNA expression levels of fibrosis markers, including *Mmp2, Col3a1*, *Tgfb1* and *Col1a1*, were also elevated in *Vsir*$^{-/-}$ mice compared to WT mice (Figure 4K). Taken together, these findings support the idea that *Vsir* deficiency promotes the development of PF.

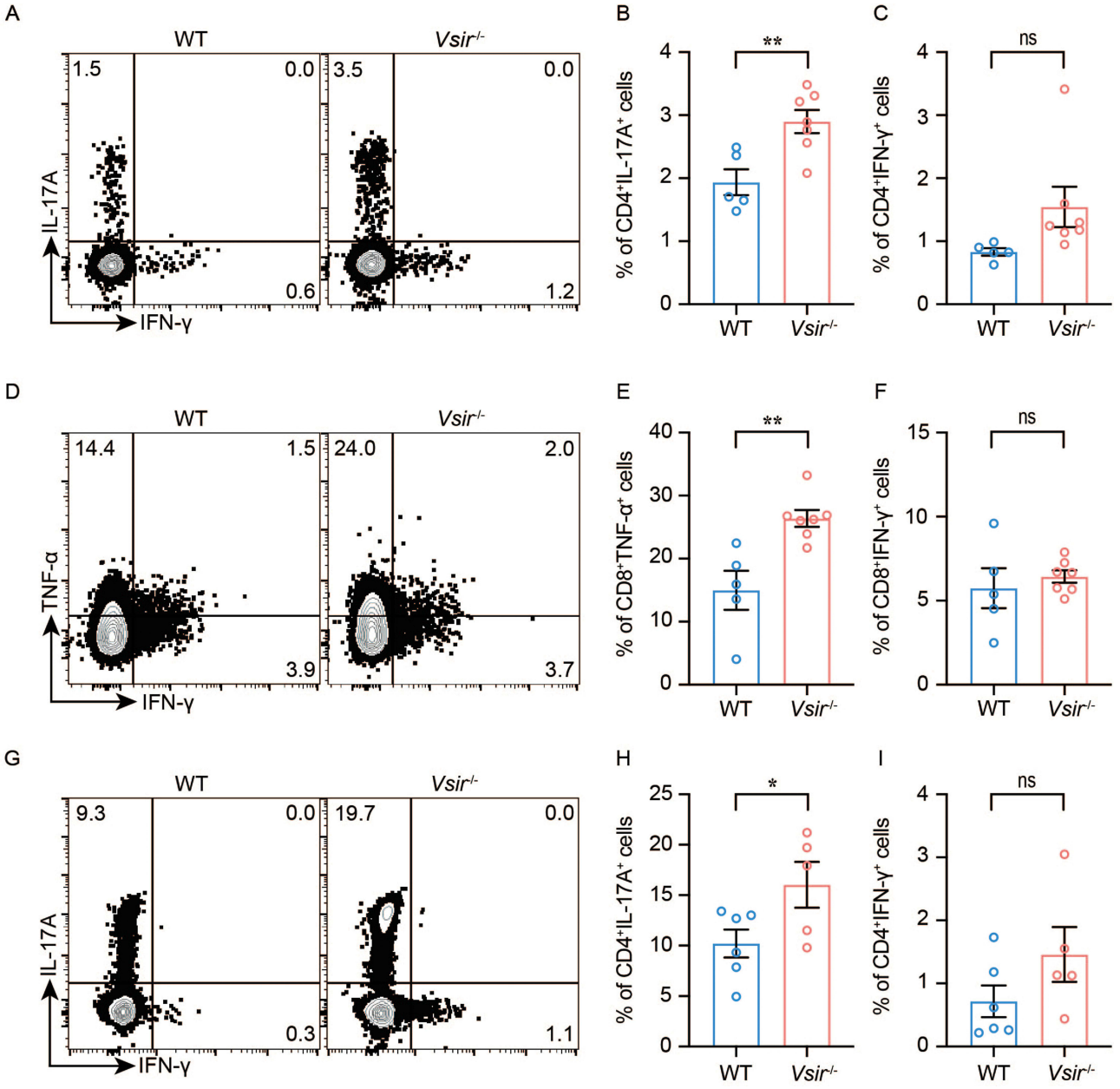

Figure 5 CD4 T cells towards Th17 is enhanced in *Vsir* deficient mice during BLM-induced lung fibrosis. (**A**–**F**) Flow cytometry analysis of single cell suspensions from draining lymph nodes (n = 5 in isotype WT group, n = 7 in *Vsir*$^{-/-}$ group). Typical gating strategies of cytokines expressions in CD4 T cells (**A**) and CD8 T cells (**D**). Cytokines IL-17A and IFN-γ expression levels in CD4 T cells were listed (**B** and **C**). TNF-α and IFN-γ levels in CD8 T cells were shown (**E** and **F**). (**G**–**I**) Flow cytometry analysis of lung single cells (n = 6 in isotype WT group, n = 5 in *Vsir*$^{-/-}$ group). Representative images of gating strategies (**G**). Cytokines IL-17A and IFN-γ expression levels in CD4 T cells were compared (**H** and **I**). Data are mean ± SEM. *$p < 0.05$, **$p < 0.01$ by Student's *t* test.

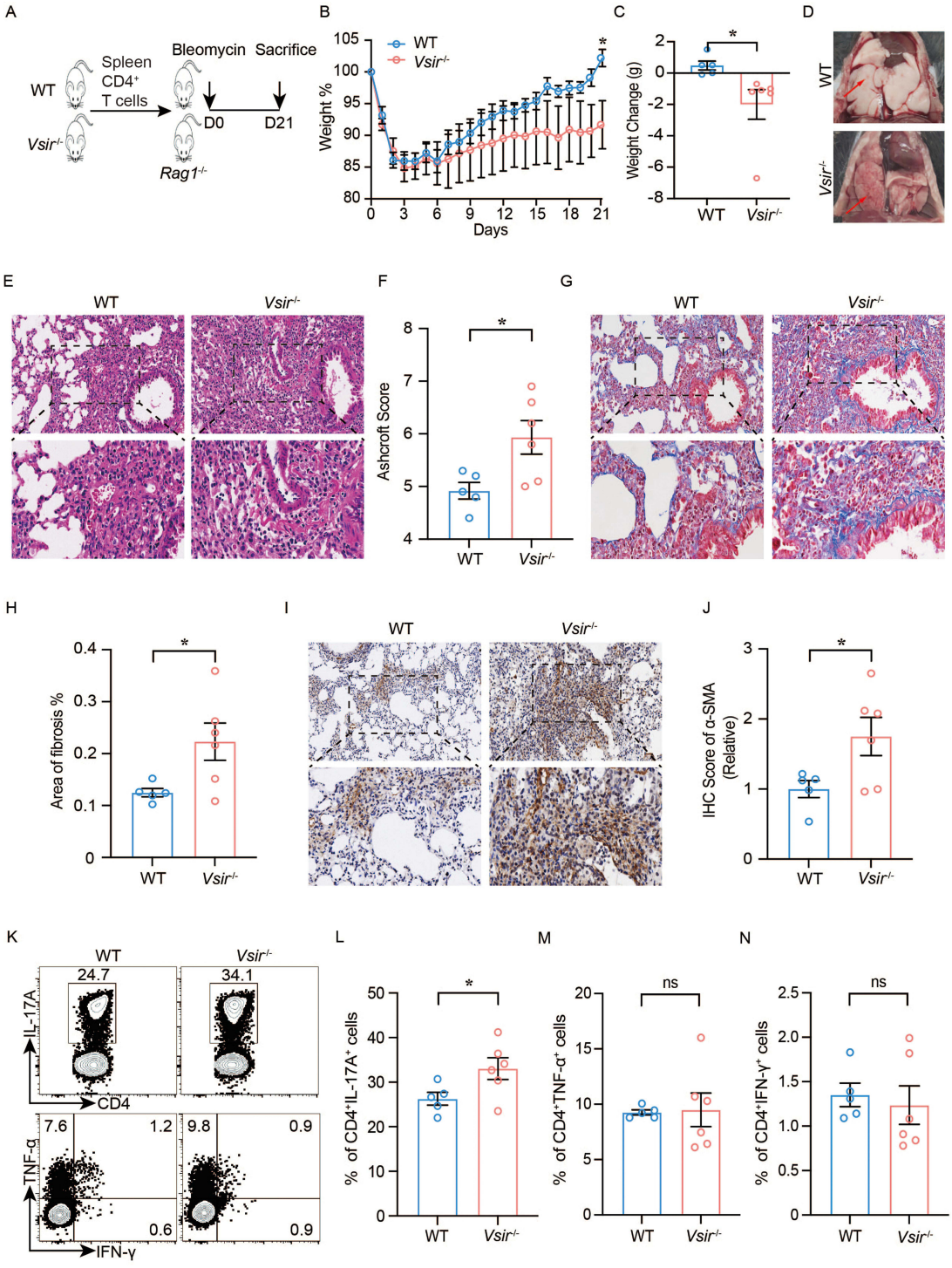

Figure 6 *Vsir*-deleted CD4 T cells exacerbate PF. (**A**) Schematic graph of murine model. CD4 T cells from WT mice and *Vsir*$^{-/-}$ mice were transferred into *Rag1*$^{-/-}$ mice. *Rag1*$^{-/-}$ mice then received single intratracheal injection of BLM two weeks after transfer, and were sacrificed at day 21 (n = 5 in WT group, n = 6 in *Vsir*$^{-/-}$ group). (**B** and **C**) Weight changes of mice during the course of BLM-induced fibrosis (**B**), and the difference of weight changes between two groups at day 21 (**C**). (**D**) Images of lungs from mice in WT group (upper) or *Vsir*$^{-/-}$ group (lower) (The red arrow indicates the location of the lesion). (**E** and **F**) H&E staining of lung sections (**E**), and Ashcroft score of each mouse in two groups (**F**). (**G** and **H**) Masson's trichrome staining of lung sections (**G**), and the area of fibrosis (**H**). (**I** and **J**) Immunohistochemistry staining of lung sections (**I**), and relative score of α-SMA (**J**). (**K**–**N**) Flow cytometry analysis of single cell suspensions of draining lymph nodes from mice in this experiment (n = 5 in WT group, n = 6 in *Vsir*$^{-/-}$ group). Representative gating strategies for cytokines expression in CD4 T cells (**K**). Cytokines IL-17A, TNF-α and IFN-γ expression levels in CD4 T cells (**L**–**N**). Original magnification: ×20 (upper), ×40 (lower). Data are mean ± SEM. *$p < 0.05$, by Student's *t* test.

Given the fact that VISTA regulated PF negatively, we further explored the detailed impact of VISTA on CD4 T cells polarization of draining lymph nodes and murine lungs. For draining lymph nodes, flow cytometry data showed increased IL-17A production in CD4 T cells and TNF-α production in CD8 T cells (Figure 5A, B, D and E). No differences were observed in IFN-γ, TNF-α and Foxp3 production in CD4 T cells (Figure 5C, Supplementary Figure 6A), as well as IFN-γ production in CD8 T cells (Figure 5F) between WT and *Vsir*$^{-/-}$ mice. For murine lungs, data pointed out higher IL-17A expression in CD4 T cells in *Vsir*$^{-/-}$ mice (Figure 5G and H). However, there were no differences in CD4 T cells for secreting IFN-γ (Figure 5I), TNF-α and Foxp3 (Supplementary Figure 6B), as well as CD8 T cells for secreting TNF-α and IFN-γ (Supplementary Figure 6C). Conclusively, *Vsir* deficiency leads to the skewing of CD4 T cells towards IL-17A-secreting subset.

Vsir-Deleted CD4 T Cells are Capable of Inducing More Severe Lung Fibrosis

Given the fact that VISTA modulated the differentiation of CD4 T cells, we then investigated whether the loss of VISTA on CD4 T cells influenced the pathogenesis of PF. To this end, we generated an adoptive transfer murine model of PF (Figure 6A). We recorded weight changes in mice throughout the disease course and observed a temporary weight loss in two groups, followed by a gradual gain of weight in the following days (Figure 6B). However, mice received *Vsir*-deleted CD4 T cells exhibited less weight gain compared to mice received WT CD4 T cells at day 21 (Figure 6C), indicating higher disease severity in mice receiving *Vsir*-deleted CD4 T cells. Consistent with previous results, mice receiving *Vsir*-deleted CD4 T cells presented increased bleeding sites and patchy dark-red lesions compared to mice receiving WT CD4 T cells (Figure 6D). H&E and Masson's trichrome staining indicated extended fibrosis in lung sections in mice received *Vsir*-deleted CD4 T cells compared to WT group (Figure 6E–H). Furthermore, higher levels of α-SMA expression were also found in the lungs of mice received *Vsir*-deleted CD4 T cells (Figure 6I and J). Importantly, flow cytometry analysis suggested that deletion of *Vsir* in CD4 T cells led to augmented IL-17A-producing CD4 T cells in draining lymph nodes. However, no differences were noted regarding the production of TNF-α and IFN-γ between *Vsir*-deleted CD4 T cells and WT CD4 T cells (Figure 6K–N). These findings further confirm the important role of VISTA in Th17 differentiation and deletion of *Vsir* in CD4 T cells promotes BLM-induced lung fibrosis by enhancing Th17 differentiation.

Discussion

The adaptive immune system is involved in the pathogenesis of PF, but the underlying mechanisms remain unclear. This study showed that VISTA was downregulated on CD4 T cells from patients with CTD-ILD. In addition, the expression of VISTA on CD4 T cells was positively correlated with pulmonary function parameters. In BLM-induced PF murine models, blockade of VISTA promoted Th17 cell differentiation and enhanced PF. Moreover, knockout of *Vsir* led to increased Th17 cells in the lungs, resulting in worsened PF. *Vsir*-deleted CD4 cells were prone to differentiate into Th17 cells and induced more severe PF than WT CD4 T cells. This study has linked VISTA to Th17 differentiation, identifying the important role of VISTA in modulating the development of PF.

In the current study, RNA-seq analysis suggested decreased *VSIR* mRNA in IPF patients compared to HCs. We also discovered decreased VISTA expression on CD4 T cells from CTD-ILD patients, and the relevance between CD4^{+}VISTA^{+} T cells and lung function parameters. Due to the involvement of the immune system in the development and progression of PF, we hypothesized that the expression of VISTA on CD4 T cells may be involved in the pathogenesis of PF. We established a PF murine model through a single-dose intratracheal instillation of BLM. The results indicated that both antagonistic blockade of VISTA and deletion of *Vsir* deteriorated the formation and progression of PF. Previous study reported that VISTA could play a role in limiting lung inflammation and fibrosis,[40] but the underlying mechanism was not reported. Here, we showed that VISTA controls the development and progression of PF by modulating Th17 differentiation. Instead of using global knockout mice, we transferred *Vsir*-deleted and WT CD4 T cells to *Rag1*$^{-/-}$ mice to investigate the specific function of VISTA on CD4 T cells during the inducing of lung fibrosis. Our data unveiled that the loss of *Vsir* on CD4 T cells promoted Th17 differentiation and exacerbated PF. Our data not only demonstrated the role of VISTA in PF but also uncovered the novel mechanism that VISTA as an important regulator for Th17 differentiation.

Research data revealed that injured epithelium and activated immune system ultimately contribute to the recruitment and abnormal activation of fibroblasts.[41] Abnormal proliferation, dysregulated apoptosis, and abnormal senescence of

fibroblasts were emphasized during the process of PF,[42] and multiple mediators were involved in activating fibroblasts.[33,43,44] IL-17 family consists of six members (IL-17A-IL-17F) and five receptors (IL-17RA-IL-17RE),[45] among which IL-17A is most widely explored in fibrosis. Levels of IL-17A and its receptor were increased in response to liver injury, and IL-17A promoted liver fibrosis by activating hepatic stellate cells.[46] Additionally, IL-17A expedited myofibroblast differentiation by enhancing IL-6 production from cardiac fibroblasts, subsequently promoting cardiac injury and fibrosis in hypertension.[47] Up-regulated IL-17A contributed to the production of ECM and profibrotic factors by activating renal fibroblasts.[48] Consistently, we showed that IL-17A activated fibroblasts into myofibroblasts and ultimately promoted the formation and development of PF effectively.

The normal functions of T cells are crucial for the body's defense and clearance of pathogens, while negative immune checkpoint molecules play a significant role in the activation, proliferation, and differentiation processes of T cells.[15] Studies indicated that VISTA expression on resting CD4 T cells downregulates T cell activation.[28,29] CD4 T cells from *Vsir*$^{-/-}$ mice exhibited significantly enhanced activation upon antigen stimulation. Further, CD4 T cell-mediated acute hepatitis was resolved after VISTA agonism.[24] Previous researches also indicated that down-regulated VISTA expression facilitated Th17 lineage differentiation.[49,50] Our results showed that both antagonistic blockade of VISTA and deletion of *Vsir* promoted CD4 T cell differentiation into Th17 cell. Moreover, CD4 T cells from *Vsir*$^{-/-}$ mice accelerated PF progression by secreting higher levels of IL-17A.

In conclusion, our study unravels a critical, previously unrecognized role of VISTA on CD4 T cells in the pathogenesis of PF. Mechanistically, VISTA on CD4 T cells negatively regulates Th17 differentiation and thus plays a protective role in the development of PF. Convincingly, our study provides mechanistic insight into the pathogenesis of PF and uncovers that therapeutic targeting VISTA could be an innovative approach against PF.

Data Sharing Statement

The data supporting the findings of this study can be obtained from the corresponding author according to reasonable request, and the corresponding author/s can be directly contacted for further inquiry.

Acknowledgment

This work is supported by the National Natural Science Foundation of China (81971519, 82171770). Graphical abstract was created with BioRender.com.

Disclosure

The authors declare that they have no known competing financial interests or personal relationships that could have appeared to influence the work reported in this paper.

References

1. Wijsenbeek M, Cottin V. Spectrum of fibrotic lung diseases. *N Engl J Med*. 2020;383:958–968. doi:10.1056/NEJMra2005230
2. Moss BJ, Ryter SW, Rosas IO. Pathogenic mechanisms underlying idiopathic pulmonary fibrosis. *Annu Rev Pathol Mech Dis*. 2022;17:515–546. doi:10.1146/annurev-pathol-042320-030240
3. Celada LJ, Kropski JA, Herazo-Maya JD, et al. PD-1 up-regulation on CD4+ T cells promotes pulmonary fibrosis through STAT3-mediated IL-17A and TGF-β1 production. *Sci Transl Med*. 2018;10:eaar8356. doi:10.1126/scitranslmed.aar8356
4. Tiringer K, Treis A, Fucik P, et al. A Th17- and Th2-skewed cytokine profile in cystic fibrosis lungs represents a potential risk factor for Pseudomonas aeruginosa infection. *Am J Respir Crit Care Med*. 2013;187:621–629. doi:10.1164/rccm.201206-1150OC
5. Zhang J, Wang D, Wang L, et al. Profibrotic effect of IL-17A and elevated IL-17RA in idiopathic pulmonary fibrosis and rheumatoid arthritis-associated lung disease support a direct role for IL-17A/IL-17RA in human fibrotic interstitial lung disease. *Am J Physiol Lung Cell Mol Physiol*. 2019;316:L487–L497. doi:10.1152/ajplung.00301.2018
6. Wilson MS, Madala SK, Ramalingam TR, et al. Bleomycin and IL-1beta-mediated pulmonary fibrosis is IL-17A dependent. *J Exp Med*. 2010;207:535–552. doi:10.1084/jem.20092121
7. Ramstein J, Broos CE, Simpson LJ, et al. IFN-γ–Producing T-Helper 17.1 cells are increased in sarcoidosis and are more prevalent than T-Helper Type 1 Cells. *Am J Respir Crit Care Med*. 2016;193:1281–1291. doi:10.1164/rccm.201507-1499OC
8. Fischer A, Ellinghaus D, Nutsua M, et al. GenPhenReSa consortium, identification of immune-relevant factors conferring sarcoidosis genetic risk. *Am J Respir Crit Care Med*. 2015;192:727–736. doi:10.1164/rccm.201503-0418OC
9. Gasse P, Riteau N, Vacher R, et al. IL-1 and IL-23 mediate early IL-17A production in pulmonary inflammation leading to late fibrosis. *PLoS One*. 2011;6:e23185. doi:10.1371/journal.pone.0023185

10. Mi S, Li Z, Yang H-Z, et al. Blocking IL-17A promotes the resolution of pulmonary inflammation and fibrosis via TGF-beta1-dependent and -independent mechanisms. *J Immunol*. 2011;187:3003–3014. doi:10.4049/jimmunol.1004081
11. Liu H, Mi S, Li Z, Hua F, Hu Z-W. Interleukin 17A inhibits autophagy through activation of PIK3CA to interrupt the GSK3B-mediated degradation of BCL2 in lung epithelial cells. *Autophagy*. 2013;9:730–742. doi:10.4161/auto.24039
12. Evrard M, Mackay LK. The highs and lows of CD4+ tissue-resident T cells in lung fibrosis. *Nat Immunol*. 2019;20:1416–1418. doi:10.1038/s41590-019-0501-3
13. Atamas SP, Fontenot AP. Regulatory T cells and lung fibrosis: a good cell gone bad. *Am J Respir Crit Care Med*. 2011;184:1224–1226. doi:10.1164/rccm.201108-1572ED
14. Sikkeland LIB, Qiao S-W, Ueland T, et al. Lung CD4+ T-cells in patients with lung fibrosis produce pro-fibrotic interleukin-13 together with interferon-γ. *Eur Respir J*. 2021;57:2000983. doi:10.1183/13993003.00983-2020
15. Qin S, Xu L, Yi M, Yu S, Wu K, Luo S. Novel immune checkpoint targets: moving beyond PD-1 and CTLA-4. *Mol Cancer*. 2019;18:155. doi:10.1186/s12943-019-1091-2
16. Zhu B, Tang L, Chen S, et al. Targeting the upstream transcriptional activator of PD-L1 as an alternative strategy in melanoma therapy. *Oncogene*. 2018;37:4941–4954. doi:10.1038/s41388-018-0314-0
17. Yu X, Harden K, Gonzalez LC, et al. The surface protein TIGIT suppresses T cell activation by promoting the generation of mature immunoregulatory dendritic cells. *Nat Immunol*. 2009;10:48–57. doi:10.1038/ni.1674
18. Lozano E, Dominguez-Villar M, Kuchroo V, Hafler DA. The TIGIT/CD226 Axis Regulates Human T Cell Function. *J Immunol*. 2012;188:3869–3875. doi:10.4049/jimmunol.1103627
19. Chocarro L, Blanco E, Zuazo M, et al. Understanding LAG-3 Signaling. *Int J Mol Sci*. 2021;22:5282. doi:10.3390/ijms22105282
20. ElTanbouly MA, Croteau W, Noelle RJ, Lines JL. Vista: a novel immunotherapy target for normalizing innate and adaptive immunity. *Semin Immunol*. 2019;42:101308. doi:10.1016/j.smim.2019.101308
21. ElTanbouly MA, Schaafsma E, Noelle RJ, Lines JL. Vista: coming of age as a multi-lineage immune checkpoint. *Clin Exp Immunol*. 2020;200:120–130. doi:10.1111/cei.13415
22. Tagliamento M, Bironzo P, Novello S. New emerging targets in cancer immunotherapy: the role of Vista. *ESMO Open*. 2019;4:e000683. doi:10.1136/esmoopen-2020-000683
23. Im E, Sim DY, Lee H-J, et al. Immune functions as a ligand or a receptor, cancer prognosis potential, clinical implication of Vista in cancer immunotherapy. *Semin Cancer Biol*. 2022;86:1066–1075. doi:10.1016/j.semcancer.2021.08.008
24. Flies DB, Han X, Higuchi T, et al. Coinhibitory receptor PD-1H preferentially suppresses $CD4^+$ T cell-mediated immunity. *J Clin Invest*. 2014;124:1966–1975. doi:10.1172/JCI74589
25. Liu H, Li X, Hu L, et al. A crucial role of the PD-1H coinhibitory receptor in suppressing experimental asthma. *Cell Mol Immunol*. 2018;15:838–845. doi:10.1038/cmi.2017.16
26. Flies DB, Wang S, Xu H, Chen L. Cutting edge: a monoclonal antibody specific for the programmed death-1 homolog prevents graft-versus-host disease in mouse models. *J Immunol*. 2011;187:1537–1541. doi:10.4049/jimmunol.1100660
27. Ceeraz S, Sergent PA, Plummer SF, et al. Vista deficiency accelerates the development of fatal murine lupus nephritis. *Arthritis Rheumatol Hoboken NJ*. 2017;69:814–825. doi:10.1002/art.40020
28. Wang L, Le Mercier I, Putra J, et al. Disruption of the immune-checkpoint Vista gene imparts a proinflammatory phenotype with predisposition to the development of autoimmunity. *Proc Natl Acad Sci U S A*. 2014;111:14846–14851. doi:10.1073/pnas.1407447111
29. Flies DB, Higuchi T, Chen L. Mechanistic assessment of PD-1H coinhibitory receptor-induced T cell tolerance to allogeneic antigens. *J Immunol*. 2015;194:5294–5304. doi:10.4049/jimmunol.1402648
30. ElTanbouly MA, Zhao Y, Nowak E, et al. Vista is a checkpoint regulator for naïve T cell quiescence and peripheral tolerance. *Science*. 2020;367:eaay0524. doi:10.1126/science.aay0524
31. Tanner L, Single AB, Bhongir RKV, et al. Small-molecule-mediated OGG1 inhibition attenuates pulmonary inflammation and lung fibrosis in a murine lung fibrosis model. *Nat Commun*. 2023;14:643. doi:10.1038/s41467-023-36314-5
32. Hübner R-H, Gitter W, El Mokhtari NE, et al. Standardized quantification of pulmonary fibrosis in histological samples. *BioTechniques*. 2008;44:507–511, 514–517. doi:10.2144/000112729
33. Liu -S-S, Liu C, Lv X, et al. The chemokine CCL1 triggers an AMFR-SPRY1 pathway that promotes differentiation of lung fibroblasts into myofibroblasts and drives pulmonary fibrosis. *Immunity*. 2021;54:2042–2056.e8. doi:10.1016/j.immuni.2021.06.008
34. Williams LM, McCann FE, Cabrita MA, et al. Identifying collagen VI as a target of fibrotic diseases regulated by CREBBP/EP300. *Proc Natl Acad Sci*. 2020;117:20753–20763. doi:10.1073/pnas.2004281117
35. Yang D, Chen X, Wang J, et al. Dysregulated lung commensal bacteria drive Interleukin-17B production to promote pulmonary fibrosis through their outer membrane vesicles. *Immunity*. 2019;50:692–706.e7. doi:10.1016/j.immuni.2019.02.001
36. Cui Z, Liao J, Cheong N, et al. The receptor for hyaluronan-mediated motility (CD168) promotes inflammation and fibrosis after acute lung injury. *Matrix Biol J Int Soc Matrix Biol*. 2019;78–79:255–271. doi:10.1016/j.matbio.2018.08.002
37. Sun P, Li L, Zhao C, Pan M, Qian Z, Su X. Deficiency of α7 nicotinic acetylcholine receptor attenuates bleomycin-induced lung fibrosis in mice. *Mol Med*. 2017;23:34–49. doi:10.2119/molmed.2016.00083
38. Burgy O, Wettstein G, Bellaye PS, et al. Deglycosylated bleomycin has the antitumor activity of bleomycin without pulmonary toxicity. *Sci Transl Med*. 2016;8:326ra20. doi:10.1126/scitranslmed.aad7785
39. Verleden SE, Tanabe N, McDonough JE, et al. Small airways pathology in idiopathic pulmonary fibrosis: a retrospective cohort study. *Lancet Respir Med*. 2020;8:573–584. doi:10.1016/S2213-2600(19)30356-X
40. Kim S-H, Adams TS, Hu Q, et al. Vista (PD-1H) is a crucial immune regulator to limit pulmonary fibrosis. *Am J Respir Cell Mol Biol*. 2023;69:22–33. doi:10.1165/rcmb.2022-0219OC
41. Li R, Jia Y, Kong X, Nie Y, Deng Y, Liu Y. Novel drug delivery systems and disease models for pulmonary fibrosis. *J Control Release off J Control Release Soc*. 2022;348:95–114. doi:10.1016/j.jconrel.2022.05.039
42. Desai O, Winkler J, Minasyan M, Herzog EL. The role of immune and inflammatory cells in idiopathic pulmonary fibrosis. *Front Med*. 2018;5:43. doi:10.3389/fmed.2018.00043

43. Geng Y, Li L, Yan J, et al. PEAR1 regulates expansion of activated fibroblasts and deposition of extracellular matrix in pulmonary fibrosis. *Nat Commun*. 2022;13:7114. doi:10.1038/s41467-022-34870-w
44. Kasam RK, Ghandikota S, Soundararajan D, et al. Inhibition of Aurora Kinase B attenuates fibroblast activation and pulmonary fibrosis. *EMBO Mol Med*. 2020;12:e12131. doi:10.15252/emmm.202012131
45. Amatya N, Garg AV, Gaffen SL. IL-17 signaling: the yin and the yang. *Trends Immunol*. 2017;38:310–322. doi:10.1016/j.it.2017.01.006
46. Meng F, Wang K, Aoyama T, et al. Interleukin-17 signaling in inflammatory, Kupffer cells, and hepatic stellate cells exacerbates liver fibrosis in mice. *Gastroenterology*. 2012;143:765–776.e3. doi:10.1053/j.gastro.2012.05.049
47. Li Y, Wu Y, Zhang C, et al. Du, γδT Cell-derived interleukin-17A via an interleukin-1β-dependent mechanism mediates cardiac injury and fibrosis in hypertension. *Hypertens Dallas Tex*. 2014;64:305–314. doi:10.1161/HYPERTENSIONAHA.113.02604
48. Weng C-H, Li Y-J, Wu -H-H, et al. Interleukin-17A induces renal fibrosis through the ERK and Smad signaling pathways. *Biomed Pharmacother*. 2020;123:109741. doi:10.1016/j.biopha.2019.109741
49. Zhang Y, Zhang X, Han J, et al. Downregulated Vista enhances Th17 differentiation and aggravates inflammation in patients with acute-on-chronic liver failure. *Hepatol Int*. 2023;17:1000–1015. doi:10.1007/s12072-023-10505-0
50. Hid Cadena R, Reitsema RD, Huitema MG, et al. Decreased expression of negative immune checkpoint vista by CD4+ T Cells Facilitates T Helper 1, T Helper 17, and T follicular helper lineage differentiation in GCA. *Front Immunol*. 2019;10:1638. doi:10.3389/fimmu.2019.01638